

Effects of heat treatment on the activated flux TIG-welded AZ31 magnesium alloy joints

Mengbing Zhou¹ · Jun Shen¹ · Dan Hu¹ · Runhua Gao¹ · Shizeng Li¹

Received: 7 November 2016 / Accepted: 28 March 2017 / Published online: 7 May 2017
© Springer-Verlag London 2017

Abstract The effects of heat treatment on the microstructures and mechanical properties of tungsten inert gas-welded AZ31 magnesium alloy joints with Cr₂O₃ flux coating were investigated by microstructural observations, microhardness, and tensile tests. The results showed that the activating flux of Cr₂O₃ improved the weld penetration and the depth/width ratio of the tungsten inert gas-welded AZ31 magnesium alloy joints markedly. Heat treatment (1) eliminated the coarsened network-like β -Mg₁₇(Al, Zn)₁₂ particles which formed in activating tungsten inert gas and (2) resulted in more uniform grain size distribution of partially melted zone. Apart from that, either the microhardness of the seams, the ultimate tensile strength, or the elongation of the welded joints was improved by aging treatment, while too high aging temperature would give rise to a sharply decreased ultimate tensile strength.

Keywords Magnesium alloys · Tungsten inert gas welding · Aging · Microstructure · Mechanical property

1 Introduction

Recently, considerable attention has been given to magnesium alloys because of their high specific strength, which makes them particularly attractive for aerospace, automobile, and other fields [1]. Many welding processes, such as tungsten

inert gas (TIG) welding [2], laser beam welding (LBW) [3], electron beam welding (EBW) [4], and friction stir welding (FSW) [5], have been applied to magnesium alloys. TIG welding is widely used for magnesium alloys due to the good weld appearance and high quality of TIG-welded joints. However, the relatively shallow penetration and low mechanical properties in single-pass TIG welding highly restricted their application in industry.

In order to improve the penetration of TIG-welded workpieces, activated tungsten inert gas (A-TIG) welding based on various oxides, halides, and metal powder compounds has been used as activating flux. This technique was a new type of welding process that adds a thin activating flux on the top surface of the base material (BM) before TIG welding [6, 7]. Currently, the widely accepted mechanism of increasing weld penetration includes surface tension theory and “arc constriction” [8–10]. Moreover, the mechanical properties of welded joints decreased due to the coarsened β -Mg₁₇(Al, Zn)₁₂ intermetallic compound (IMC) in the fusion zone (FZ) of A-TIG weld joints and they distributed at the α -Mg grain boundaries and then formed as a network-like structure in the case of the flux coating [10]. A partial melting zone (PMZ) was formed at the adjacent of the complete fusion boundary due to that the metal in the area was heated to a temperature range between the liquidus and eutectic temperature, which is a major technical problem for decreasing the mechanical properties of welded joints [11, 12].

Usually, the PMZ could be solved by the heat treatment after welding [13–15]. However, the investigation about the effects of heat treatment on microstructures and mechanical properties of A-TIG-welded magnesium alloy joints was limited. In this paper, the Cr₂O₃ was used as the activating flux. After welding, solution and aging treatments were carried out on A-TIG-welded AZ31 magnesium alloy joints. The influences of the heat treatment on the microstructural and

✉ Jun Shen
shenjun@cqu.edu.cn

¹ State Key Laboratory of Mechanical Transmission, College of Material Science & Engineering, Chongqing University, Chongqing 400044, People's Republic of China

Table 1 The nominated chemical composition of AZ31 magnesium alloy

| Al | Zn | Mn | Si | Cu | Ni | Fe | Mg |
|------|------|------|------|-------|--------|--------|---------|
| 3.27 | 0.91 | 0.25 | <0.1 | <0.05 | <0.005 | <0.005 | Balance |

mechanical property evolution of the A-TIG-welded AZ31 magnesium alloy joints with Cr₂O₃ activating flux were detail studied.

2 Materials and methods

Hot-extruded AZ31 magnesium alloy plates, with a dimension of 100 mm × 100 mm × 5 mm, were butt-welded by the AC automatic welding machine (NSA-500-1) in the work-hardened condition. The nominated chemical composition of the AZ31 magnesium alloy is collected in Table 1. The surfaces of the plates were cleaned with acetone to eliminate surface contamination before welding. Cr₂O₃ powder was selected as a flux in the experiments. Before welding, a brush was used to apply the flux powders, which were dispersed uniformly in ethanol, to the top surface of each specimen with a width of about 40 mm. The surface coating density of the flux was constant ($5 \pm 0.15 \text{ mg cm}^{-2}$). The experimental parameters used in the experiment are listed in Table 2.

After welding, a solution treatment (in a heat treatment furnace, SX2-4-10) was performed on some samples at 688 K with six different times (1, 2, 3, 4, 8, and 12 h), and then, they were quenched in water. Aging treatments of samples were performed at six different aging temperatures (403, 423, 443, 463, 483, and 503 K) for 24 h after the solution treatment, respectively. And then, the surfaces of the welded seams were photographed for macroscopic morphology analysis and the cross sections of the welded seams were prepared using the standard metallographic procedures and etched in the etchant (2 g picric acid, 50 ml ethanol, 5 ml acetic acid). The penetrations and the widths of the weld seam were measured so as to achieve the depth/width (D/W) ratio of the welding joints.

The microstructures and fracture surfaces of BM and the untreated/treated welded joints were characterized by an optical microscopy (MDJ200) and a scanning electron microscopy (TESCAN VEGA II LMV SEM). Energy-dispersive X-ray spectroscopy (OXFORD, ISIS300 EDS) was used to detect

the elemental composition and help to determine the phases formed in the welded seams. Based on the quantitative stereology theory defined by Xu and Chen [16], the volume fraction (V_v) of the secondary phase formed in the welded joints was evaluated by a formula as follows:

$$V_v = A_A \quad (1)$$

where A_A is the area percentage of the secondary phase in a cross section of the welded seam. Hardness measurements were carried out by the Vickers hardness test ASTM: E384-11e1 according to the standard test method and were performed with a Vickers hardness tester (V-1000) with a load of 1000 g and a load period of 20 s. ASTM: E8/E8 M-11 guidelines were followed for preparing and testing the tensile specimens. The welded joints were machined into a form of a gauge section 15 mm long and 4 mm wide for tensile specimens, as illustrated in Fig. 1. Two types of tensile test specimens were machined from the joints: (i) BM (H specimen) and (ii) transverse specimens containing the weld in the center of the gauge length (T specimen). The tensile tests were carried out with an electronic testing machine (SANS XYA105C) at room temperature. The tensile velocity was 0.5 mm min^{-1} . Each data for the ultimate tensile strength (UTS) value represents an average of three samples under the same condition.

3 Results and discussion

3.1 Macromorphologies of the welded seams

The surface appearances and the cross-sectional outline of the fusion zone (FZ) of the seams welded with/without Cr₂O₃ flux coating are shown in Fig. 2. It was found that the welding seams of the A-TIG-welded AZ31 magnesium alloy joints exhibited smooth surface (without some visual defects). Moreover, in the A-TIG welding joints, there was a great improvement in terms of the D/W ratio, which achieved 184% of those of normal TIG welding joints.

3.2 Microstructures of the untreated welded seams

The typical microstructures of the ordinary TIG/A-TIG-welded joints are shown in Fig. 3. One can see that the microstructure of the TIG-welded joints contained BM, FZ, and heat-affected zone (HAZ) (as seen in Fig. 3a), while the microstructure of the A-TIG-welded joint included BM, FZ,

Table 2 The welding parameters in the experiment

| Welding current (A) | Welding voltage (V) | Welding speed (mm/min) | Flow rate of shielding gas (L/min) | Heat input (J/mm) |
|---------------------|---------------------|------------------------|------------------------------------|-------------------|
| 120 | 15 | 200 | 15 | 486 |

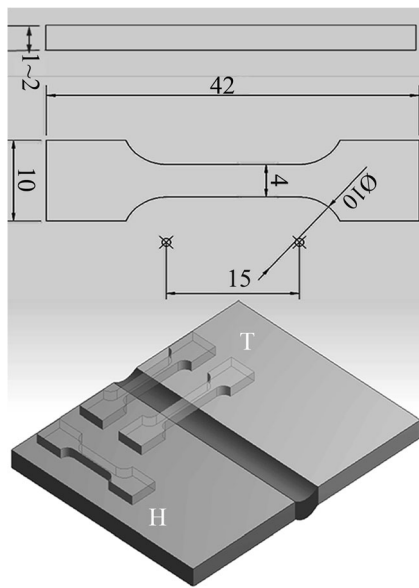


Fig. 1 Schematic drawing of the two different tensile test specimens used in the present investigation

HAZ, and PMZ (Fig. 3b). In the PMZ, the melted portion resolidified into islands of dendrites and surrounded by interdendritic eutectic. The FZ, PMZ, and HAZ are mainly composed of primary phase and secondary phase. Figure 4 shows the EDS results for the primary phase and the secondary phase in AZ31 magnesium alloy weldment. The EDS analysis results showed that the primary phase contained a large amount of Mg (97.17 at.%) element (see in Fig. 4c) while the secondary phase contained Al (27.83 at.%), Zn (11.52 at.%), and Mg (60.65 at.%) elements (see Fig. 4d). According to the Mg–Al binary phase diagram and other literatures [17, 18], the primary phase is α -Mg (marked with an arrow A in Fig. 4a, b) and the secondary phase is β -Mg₁₇(Al, Zn)₁₂ (marked with an arrow B in Fig. 4a, b). A large number of continuous and discontinuous β -Mg₁₇(Al, Zn)₁₂ particles precipitated at the α -Mg grain boundaries and also on the inside of the α -Mg grains in the FZ and PMZ of the untreated sample (as seen in Fig. 3c–e). The FZ of the ordinary TIG (Fig. 3c) and A-TIG welding joints (Fig. 3e) all exhibited equiaxed grains in the interior of the welds. The FZ of the

ordinary TIG-welded joints exhibited a finer crystal structure and a smaller β -Mg₁₇(Al, Zn)₁₂ particles compared with those of the A-TIG welding joints (as seen in Fig. 3c, e).

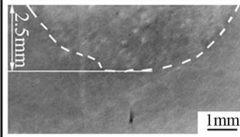
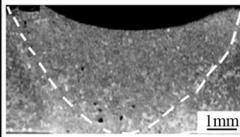
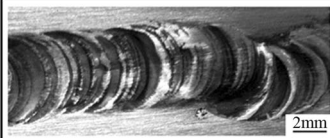

The degree of liquefaction of PMZ increased with the increase of Zn content in the BM, which can be measured with the liquid quantity. This relationship can be expressed by the formula as follows [19]:

$$f_L = \left(\frac{-C_0 m_L}{T_m - T} \right)^{1/(1-k)} \tag{2}$$

where f_L is the liquid quantity of PMZ, m_L is the slope of the liquidus, C_0 is the content of Zn, T_m is the melting point of pure metal, T is the temperature of the partially molten zone, and k is the equilibrium partition coefficient of metal. It could be seen that the f_L increased with the increasing of the C_0 , meaning that the more the Zn content in the BM, the higher the degree of liquefaction of the PMZ. Also, increasing the heat input during the welding process may increase the degree of liquefaction of the PMZ as the peak temperature and the waiting time between liquidus and eutectic temperature of the PMZ increase with the increase of welding input power. Moreover, the flux coating improved the heat input in the welding pool [9]. These suggest that a PMZ may be formed in the AZ31 magnesium alloy A-TIG welding joints.

The α -Mg grain in the FZ is finer in comparison to the PMZ and HAZ due to the higher cooling rate of the welding pool because of the high thermal conductivity of AZ31 magnesium alloy. During the welding process, the temperature in the HAZ might be up to 527 K [17]; therefore, grain coarsening might occur in the HAZ. During the TIG welding process, the solidification of the metal in the welded seam was a non-equilibrium process, so the β -Mg₁₇(Al, Zn)₁₂ particles were distributed both at the grain boundaries and on the inside of the α -Mg grains. Grain boundary and interdendritic precipitates in Mg alloys have a low melting temperature (around 723 K for β -Mg₁₇(Al, Zn)₁₂ [20] and even lower for the ternary Mg–Al–Zn eutectic). As the temperature of the base metal adjacent to the molten pool will rise above the melting temperature of the eutectic during welding, the grain interdendritic boundary precipitates and the PMZ was formed.

Fig. 2 Images of the appearances and outlines of the FZ of the TIG-welded AZ31 magnesium alloy joints with/without Cr₂O₃ flux coating

| | without flux coating | | with Cr ₂ O ₃ coating | |
|---------------------------|--|------|---|------|
| cross sectional overviews |  | D/W |  | D/W |
| | | 0.31 | | 0.57 |
| surface appearances |  | |  | |

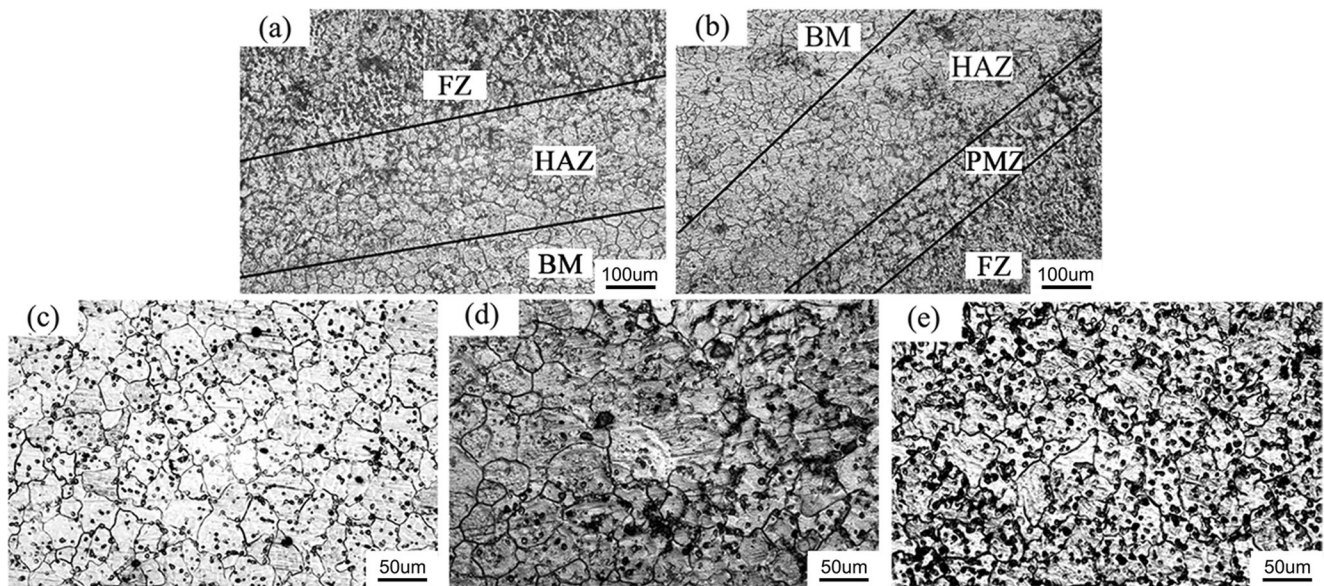


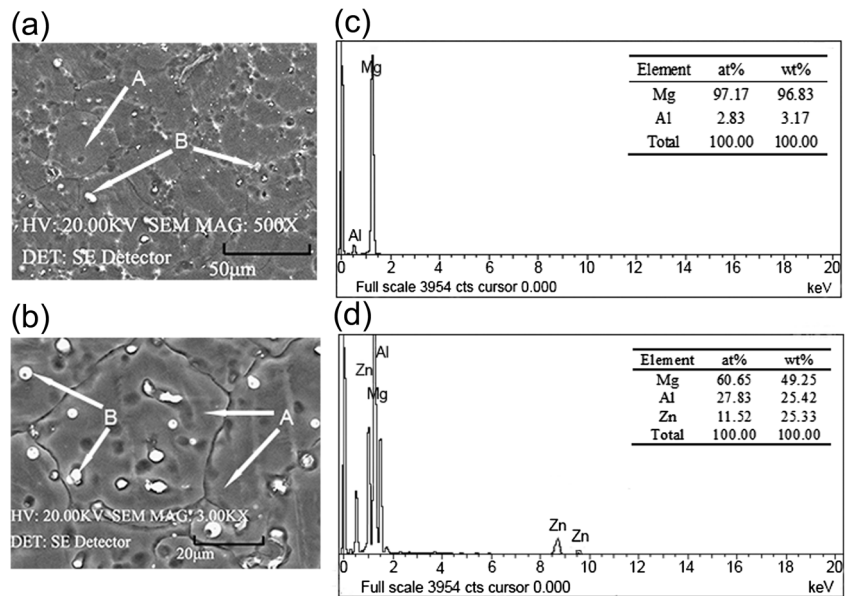
Fig. 3 The microstructures of the untreated TIG-welded AZ31 magnesium alloy joints with/without flux coating. **a** Typical microstructure of an untreated welded joint without flux coating. **b** Typical microstructure of an untreated welded joint with flux coating. **c**

FZ of an untreated welded joint without flux coating. **d** PMZ of an untreated welded joint with flux coating. **e** FZ of an untreated welded joint with flux coating

In addition, the growth of the α -Mg grains and β -Mg₁₇(Al, Zn)₁₂ particles was restrained by relatively high cooling rate of the welding pool. Compared with those of the ordinary TIG welding pool, the surface of the A-TIG welding pool had a

relatively low temperature gradient when it was covered by the Cr₂O₃ coating. Those reasons might be that the Cr₂O₃ coating suppressed the heat radiation from welding pool to the air and then decreased the temperature gradient of the

Fig. 4 The EDS results for the primary phase and the secondary phase in AZ31 magnesium alloy weldment. **a** Gray dendrites surrounded by a white zone in the PMZ can be seen, **b** SEM images of FZ, **c** EDS results of the primary phase, and **d** EDS results of the secondary phase



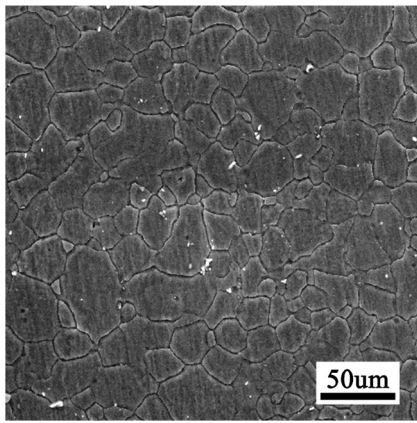


Fig. 5 The microstructure of the BM

welding pool [21]. Therefore, the lower cooling rate and longer crystallization time led to coarsened the α -Mg grains and the β -Mg₁₇(Al, Zn)₁₂ particles in the FZ of the A-TIG welding. Furthermore, due to the relatively lower cooling rate and the longer recrystallization time of the HAZ in the A-TIG welding pool, grain coarsening occurred in the HAZ. The same results also were found in the research of Liu et al. [10].

3.3 The effects of heat treatment on the welded joints

3.3.1 Microstructures of the welded seams

Figure 5 shows the microstructure of the BM; the average grain size of the BM was 29.2 μ m. Figure 6 shows the microstructure of the FZ/PMZ of the heat-treated A-TIG-welded AZ31 magnesium alloy joints. With an increased time of the

solution treatment, more β -Mg₁₇(Al, Zn)₁₂ particles dissolved into the α -Mg grains. Only small amounts of them were distributed at the grain boundaries when the samples were treated at 688 K for 3 h (as seen in Fig. 6b). The α -Mg grains coarsened sharply when the time of solution treatment was too long (Fig. 6c), while, with an increase in the aging temperature, more β -Mg₁₇(Al, Zn)₁₂ particles precipitated from the α -Mg grains and distributed at the boundaries as well as inside the α -Mg grains (Fig. 6d–f). The β -Mg₁₇(Al, Zn)₁₂ particles of FZ and PMZ of the aging-treated joints were smaller (Fig. 6d, e) than those of the untreated welded joints (Fig. 3d, e). From Fig. 6f, one can see that the β -Mg₁₇(Al, Zn)₁₂ particles of FZ coarsened seriously when the temperature was over 483 K.

Using quantitative metallographic method [22] measures the average sizes of the α -Mg grains in the FZ of the treated welded joints with/without Cr₂O₃ flux coating. The average grain size of the FZ of an untreated welded joint without flux coating was 36.2 μ m; that with flux coating was 45.3 μ m. After heat treatment, the average grain sizes were measured and the results are shown in Table 3.

3.3.2 Distribution of the microhardness of the welded seams

Figure 7 shows the distribution of the microhardness of the A-TIG-welded AZ31 magnesium alloy joints without heat treatment and aging at 483 K. The microhardness of the BM was higher than that of the FZ, the PMZ, and the HAZ, attributed to the smaller grain size of the BM. The microhardness of the joints increased obviously after 483-K aging treatment. Figure 8 shows the average microhardness of the FZ and the

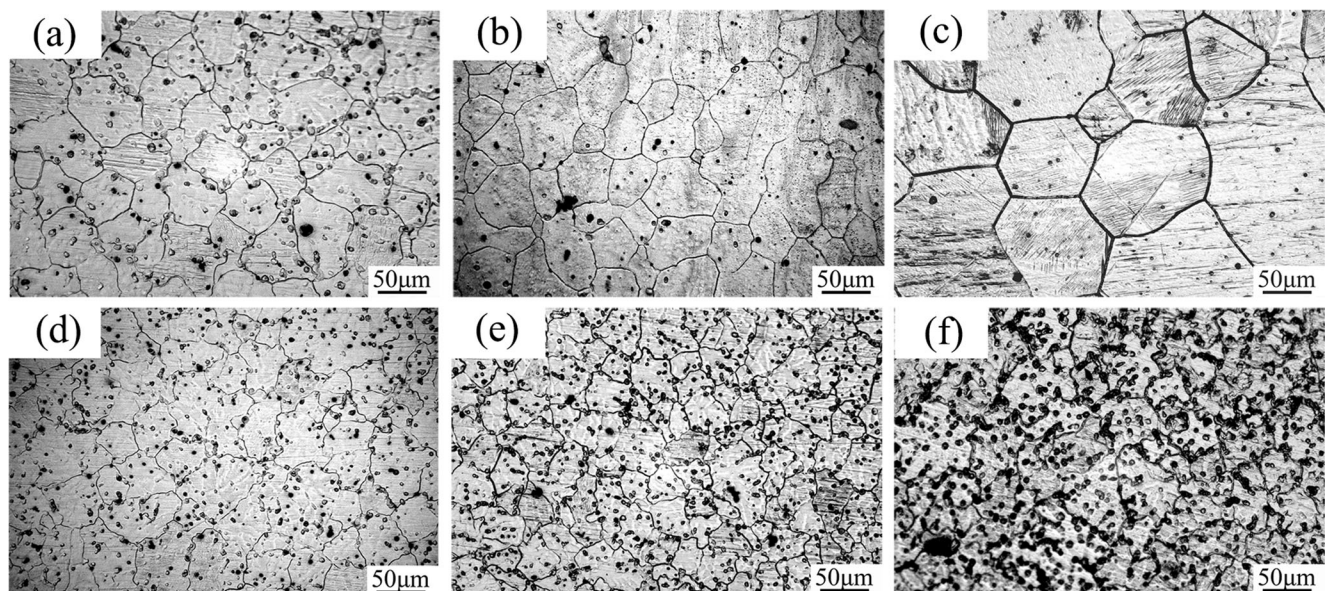


Fig. 6 The microstructures of the FZ/PMZ of the treated welded joints with Cr₂O₃ flux coating. **a** FZ of the welded joint solution-treated for 2 h. **b** FZ of the welded joint solution-treated for 3 h. **c** FZ of the welded joint

solution-treated for 12 h. **d** PMZ of the welded joint after 483-K aging treatment. **e** FZ of the welded joint after 483-K aging treatment. **f** FZ of the welded joint after 503-K aging treatment

Table 3 The average grain size of the FZ with flux coating after heat treatment

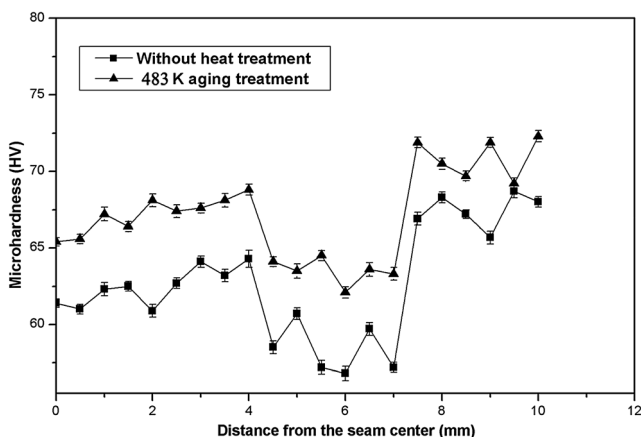
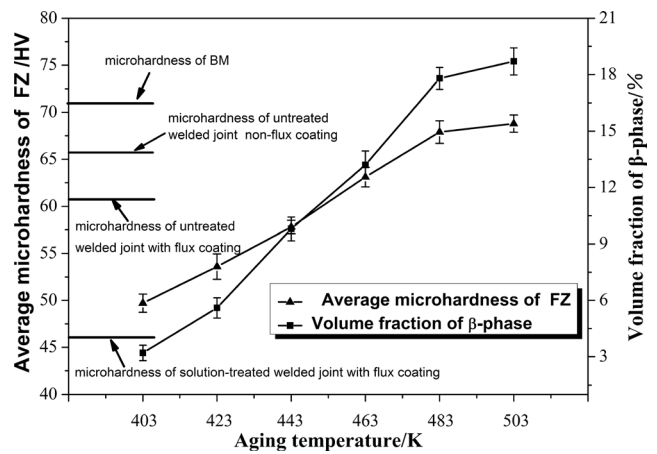
| | Solution treatment (h) | | | Aging treatment (K) | | | |
|--------------------------------|------------------------|------|-------|---------------------|------|------|------|
| | 2 | 3 | 12 | 403 | 463 | 483 | 503 |
| Average size (μm) | 44.8 | 54.6 | 106.1 | 46.2 | 49.4 | 50.1 | 58.6 |

volume fraction of the $\beta\text{-Mg}_{17}(\text{Al}, \text{Zn})_{12}$ particles in the FZ of the ordinary TIG/A-TIG welding AZ31 magnesium alloy joints. The microhardness of untreated welded joint with non-flux coating exhibiting a finer grain sizes is higher than that with flux coating, although the volume fraction of the $\beta\text{-Mg}_{17}(\text{Al}, \text{Zn})_{12}$ in the FZ of the A-TIG is larger than that of the TIG. In addition, the average microhardness of the FZ of the A-TIG-welded joints was greatly improved by the aging treatment. It increased gradually with an increase of aging temperature due to the increased volume fraction of the $\beta\text{-Mg}_{17}(\text{Al}, \text{Zn})_{12}$ particles. When the aging temperature was higher than 443 K, it was higher than that of untreated ordinary TIG/A-TIG-welded joints.

The microhardness of an alloy is affected mainly by the grain size of primary-phase and dispersed spacing of the secondary-phase particles. According to the Orowan hardening mechanism [23], the decrease in the dispersed spacing of secondary-phase particles improves the hardness of an alloy. This relationship can be expressed by the formula as follows:

$$\sigma_{\text{OR}} = \frac{0.13G_m b}{\lambda} \ln \frac{r}{b} \quad (3)$$

where G_m is the shear modulus of the alloy matrix, b is the Burgers vector, r is the dispersed radius of the $\beta\text{-Mg}_{17}(\text{Al}, \text{Zn})_{12}$ phase, which is constant, and σ_{OR} is the microhardness of the FZ. It can be seen that the average microhardness of the FZ increased with the increase of the aging temperature as the $\beta\text{-Mg}_{17}(\text{Al}, \text{Zn})_{12}$ particles in the FZ of the welded joints.

**Fig. 7** Distribution of microhardness of weld joints after 503-K aging treatment**Fig. 8** The average microhardness of the FZ of the TIG-welded AZ31 magnesium alloy joints with Cr_2O_3 flux coating

3.3.3 Tensile strength of the welded joints

Figure 9 shows the tensile test results including ultimate tensile strength (UTS) value, elongation (E), and failure location of the aging-treated ordinary TIG/A-TIG-welded AZ31 magnesium alloy joints. The mechanical properties of the BM are considerably higher than those of the welding joints. The UTS values of ordinary TIG/A-TIG welding joints were 226 MPa (86.9% of the BM (260.2 MPa)) and 211 MPa (81.2% of the BM), respectively. With the increasing aging temperature, the UTS value of the A-TIG-welded joints increased due to the increasing volume fraction and dispersed spacing of the $\beta\text{-Mg}_{17}(\text{Al}, \text{Zn})_{12}$ particles.

However, it decreased sharply when the aging temperature was too high because the $\beta\text{-Mg}_{17}(\text{Al}, \text{Zn})_{12}$ particles in the FZ coarsened and distributed at the $\alpha\text{-Mg}$ grain boundaries and formed a network-like structure. The UTS value of the A-TIG-welded joints reached the maximum value (87.7% that of the BM) when the aging temperature reached to 483 K. Moreover, the elongation of the aging-treated A-TIG-welded joints increased slightly due to an increase in the volume fraction of the $\beta\text{-Mg}_{17}(\text{Al}, \text{Zn})_{12}$ particles in the FZ (see Fig. 8). It should be pointed out that the fracture of welded joints occurred in the PMZ/HAZ when the aging temperature was lower than 483 K because this was the weakest zone in the A-TIG-welded joints of the magnesium alloy (the grain coarsening in the HAZ and the width of the HAZ increased due to the effect of the thermal cycling and flux coating). However, the fractures occurred in the FZ when the aging temperature was higher than 483 K because the network-like structure of $\beta\text{-Mg}_{17}(\text{Al}, \text{Zn})_{12}$ particles along the grain boundaries in the FZ produced local stress concentrations and the cracks may initiate at the $\beta\text{-Mg}_{17}(\text{Al}, \text{Zn})_{12}$ particles along the grain boundaries.

The microstructures of $\alpha\text{-Mg}$ phase in the weld seam preserve the effect of strengthening matrix, and the $\beta\text{-Mg}_{17}(\text{Al}, \text{Zn})_{12}$ particles maintain the solid solution strengthening effect

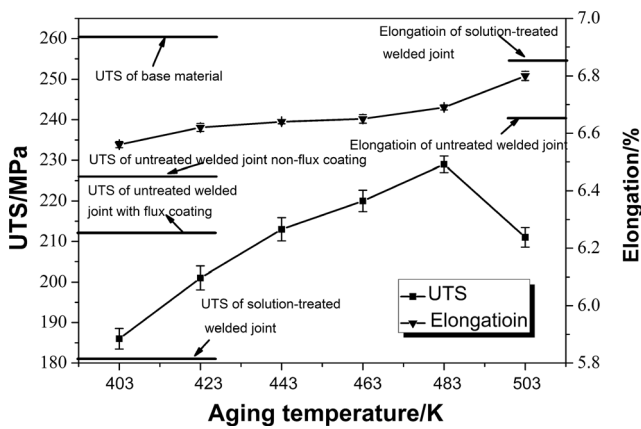


Fig. 9 The tensile test results of the ultimate tensile strength (UTS) value and elongation (E) of the TIG-welded AZ31 magnesium alloy joints with/without Cr_2O_3 flux coating

[24, 25]. Both the effects of strengthening matrix and solution strengthening benefit the mechanical properties of welded joint in the weld seam. The increase of UTS has been attributed to the increases of solution strengthening effect of $\beta\text{-Mg}_{17}(\text{Al}, \text{Zn})_{12}$ particles with increases of the aging temperature and strengthening matrix of $\alpha\text{-Mg}$ phase in the weld seams. Moreover, as increasing the value of aging temperature, the effect of strengthening matrix on the microstructures of $\alpha\text{-Mg}$ phase upgrades the ductility in the weld joints [24, 25], while the solution strengthening of $\beta\text{-Mg}_{17}(\text{Al}, \text{Zn})_{12}$ particles was enlarged with increases of the aging temperature, which results in promoting the ductility of the microstructures of $\alpha\text{-Mg}$ phase in the weld seam. However, hot extrusion generally gives rise to a strong basal texture and this also leads to a very limited ductility in BM. Consequently, the elongation of the aging-treated TIG-welded AZ31 magnesium alloy increased slightly. Higher aging temperature has the advantage of a strengthening matrix effect for the microstructures of $\alpha\text{-Mg}$ phase in the welded seam. This result is in accordance with the report of Tsai et al. [26].

SEM images of typical tensile fracture surfaces of AZ31 magnesium alloy (BM hot extruded), untreated A-TIG-welded joint, and after 483-K aging-treated A-TIG-welded joint are shown in Fig. 10. The fracture surface of the BM

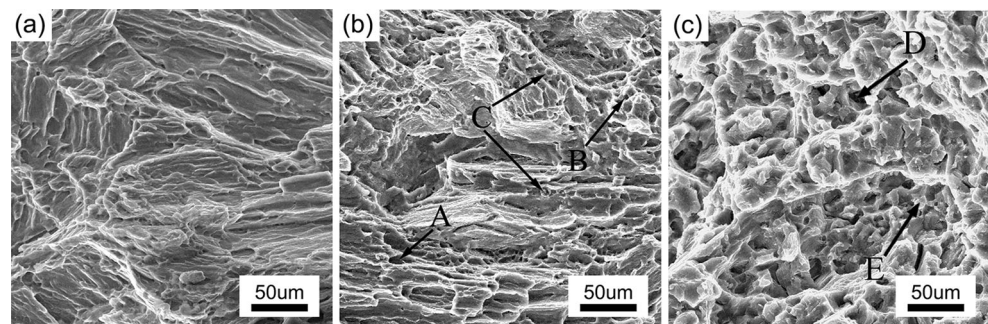
mainly exhibited the feature of a ductile fracture, which was characterized by more tearing fibers and ridges (Fig. 10a). Cleavage surfaces (marked with an arrow A in Fig. 10b), secondary cracks (marked with an arrow B in Fig. 10b) and secondary-phase particles (marked with an arrow C in the Fig. 10b), which were taken as typical brittle fracture features, could be seen on the fracture surface of the untreated A-TIG-welded joints. The fracture mechanism of the untreated A-TIG-welded AZ31 magnesium alloy joints was ductile-brittle mixed fracture. The dimples (marked with an arrow D in Fig. 10c) and secondary-phase particles (marked with an arrow E in Fig. 10c), which were taken as typical ductile fracture features, could be seen on the fracture surface of the welded joints. The feature of the fracture of the A-TIG-welded joint indicated after the 483-K aging treatment underwent ductile deformation during the tensile test, as the fine and dispersed $\beta\text{-Mg}_{17}(\text{Al}, \text{Zn})_{12}$ particles distributed both inside and at the boundaries of $\alpha\text{-Mg}$ phase in the weld seams after being aging treated at 483 K (Fig. 6). These particles can enhance the strength of both the grain interiors and their boundaries, by obstructing the dislocation annihilation and thus restricting the slip inside the grains during the tensile test.

4 Conclusions

The effects of solution and aging treatments on the microstructures and the mechanical properties of TIG-welded AZ31 magnesium alloy joints with Cr_2O_3 flux coating were investigated. The main conclusions may be summarized as follows:

1. The ordinary TIG/A-TIG welding seams exhibit smooth surface. Cr_2O_3 flux led to a great improvement in the D/W ratio of the welded joint, up to 184% compared with the normal welded seam without flux.
2. Almost all $\beta\text{-Mg}_{17}(\text{Al}, \text{Zn})_{12}$ particles dissolved into the $\alpha\text{-Mg}$ grains when the A-TIG-welded sample was treated at 688 K for 3 h. With an increase in the aging temperature, more $\beta\text{-Mg}_{17}(\text{Al}, \text{Zn})_{12}$ particles precipitated from the $\alpha\text{-Mg}$ grains. The $\beta\text{-Mg}_{17}(\text{Al}, \text{Zn})_{12}$ particles of the aging-treated A-TIG-welded joints were smaller

Fig. 10 SEM pictures of the tensile fracture surfaces of the magnesium alloy: **a** BM of hot-extruded AZ31 magnesium alloy, **b** untreated welded joint with Cr_2O_3 flux coating, and **c** after 483 K aging-treated welded joint with Cr_2O_3 flux coating



compared with those of the untreated welded joints but coarsened when the aging temperature was over 483 K.

3. The microhardness of the joints increased obviously after 483-K aging treatment. The average microhardness of the FZ of the A-TIG-welded joints was greatly improved by the aging treatment. It increased gradually with an increase in the aging temperature (higher than that of the untreated seam when the aging temperature was over 463 K) due to the increased volume fraction of the β - $Mg_{17}(Al, Zn)_{12}$ particles.
4. The aging treatment improved the UTS value and elongation of the A-TIG-welded joints. The UTS value increased with the increase in aging temperature (reached the maximum value (87.7% that of the BM) when the temperature reached to 483 K) but decreased sharply when the temperature was too high.

Acknowledgements This research is supported by a National Natural Science Foundation of China (Grant No. 51375511), a Chongqing Research Program of Basic Research and Frontier Technology (Project No. cstc2016jcyjA0167), a Science and technology project in the field of social development of Shapingba District of Chongqing (Project No. SF201602), a Key industry technology innovation fund of science and technology development board of Xiangcheng district of Suzhou (Project No. XJ201608), and a Science and technology project of Beibei district of Chongqing (Project No. 2016-27).

References

1. Westengen H (2000) Magnesium die casting: from ingots to automotive parts. *Light Metal* 58:44–52
2. Razalrose A, Manisekar K, Balasubramanian V, Rajakumar S (2012) Prediction and optimization of pulsed current tungsten inert gas welding parameters to attain maximum tensile strength in AZ61A magnesium alloy. *Mater Design* 37:334–348
3. Nasiri AM, Weckman DC, Zhou Y (2015) Interfacial microstructure of laser brazed AZ31B magnesium to Snplated steel sheet. *Weld J* 94:61–72
4. Luo Y, Ye H, Du CH, Xu HB (2012) Influence of focusing thermal effect upon AZ91D magnesium alloy weld during vacuum electron beam welding. *Vacuum* 86:1262–1267
5. Pan FS, Xu AL, Deng D, Ye JH, Jiang XQ, Tang A, Ran Y (2016) Effects of friction stir welding on microstructure and mechanical properties of magnesium alloy Mg-5Al-3Sn. *Mater Design* 110:266–274
6. Tathgir S, Bhattacharya A, Bera TK (2015) Influence of current and shielding gas in TiO₂ flux activated TIG welding on different graded steels. *Mater Manuf Process* 30:1115–1123
7. Tathgir S, Bhattacharya A (2016) Activated-TIG welding of different steels: influence of various flux and shielding gas. *Mater Manuf Process* 31:335–342
8. Modenesi PJ, Neto PC, Apolinário ER, Dias KB (2015) Effect of flux density and the presence of additives in ATIG welding of austenitic stainless steel. *Weld Int* 29:425–432
9. Li QM, Wang XH, Zou ZD, Wu J (2007) Effect of activating flux on arc shape and arc voltage in tungsten inert gas welding. *T Nonfer Metal Soc* 17:486–490
10. Liu FY, Yang CL, Lin SB, Wu L, Su S (2003) Effect of weld microstructure on weld properties in A-TIG welding of titanium alloy. *T Nonfer Metal Soc* 13:876–880
11. Li Q, Wu AP, Li YJ, Wang GQ, Yan DY, Liu J (2015) Influence of temperature cycles on the microstructures and mechanical properties of the partially melted zone in the fusion welded joints of 2219 aluminum alloy. *Mater Sci Eng A* 623:38–48
12. Stern A, Munitz A (1999) Partially melted zone microstructural characterization from gas tungsten-arc bead on plate welds of magnesium AZ91 alloy. *J Mater Sci Lett* 18:853–855
13. Peng D, Shen J, Tang Q, Wu CP, Zhou YB (2013) Effects of aging treatment and heat input on the microstructures and mechanical properties of TIG-welded 6061-T6 alloy joints. *Int J Miner Metal Mater* 20:259–265
14. Sharma C, Dwivedi DK, Kumar P (2013) Effect of post weld heat treatments on microstructure and mechanical properties of friction stir welded joints of Al-Zn-Mg alloy AA7039. *Mater Design* 43:134–143
15. Ramkumar KD, Ramanand R, Ameer A, Aghil KS, Arivazhagan N (2016) Effect of post weld heat treatment on the microstructure and tensile properties of activated flux TIG welds of Inconel X750. *Mater Sci Eng A* 658:326–338
16. Xu JL, Chen C (2004) The research of materials microstructure analysis. *Acta Metrologica Sinica* 25:369–373
17. Liang GL, Yuan SQ (2008) Study on the temperature measurement of AZ31B magnesium alloy in gas tungsten arc welding. *Mater Lett* 62:2282–2284
18. Liu LM, Dong CF (2006) Gas tungsten-arc filler welding of AZ31 magnesium alloy. *Mater Lett* 60:2194–2197
19. Kou S (2002) *Welding metallurgy*, 2nd edn. Wiley-Interscience, Hoboken
20. Villars P, Prince A, Okamoto H (1990) *Handbook of ternary alloy phase diagrams*. American Society for Metals, Metals Park
21. Wang L, Shen J, Xu N (2011) Effects of TiO₂ coating on the microstructures and mechanical properties of tungsten inert gas welded AZ31 magnesium alloy joints. *Mater Sci Eng A* 528:7276–7284
22. Kupczyk J (2006) Application of significance tests in quantitative metallographic analysis of a C-Mn-B steel 81: 171–175
23. Zhang Z, Chen DL (2006) Consideration of Orowan strengthening effect in particulate-reinforced metal matrix nanocomposites: a model for predicting their yield strength. *Scripta Mater* 54:1321–1326
24. Feng YQ, Li Y, Luo Z, Ling ZX, Wang ZM (2016) Resistance spot welding of Mg to electro-galvanized steel with hot-dip galvanized steel interlayer. *J Mater Process Tech* 236:114–122
25. Wang LF, Mostaed E, Cao XQ, Huang GS, Fabrizi A, Bonollo F, Chi CZ, Vedani M (2016) Effects of texture and grain size on mechanical properties of AZ80 magnesium alloys at lower temperatures. *Mater Design* 89:1–8
26. Tsai TC, Chou CC, Tsai DM, Chiang KT (2011) Chiang modeling and analyzing the effects of heat treatment on the characteristics of magnesium alloy joint welded by the tungsten-arc inert gas welding. *Mater Design* 32:4187–4194